^{40}Ar/^{39}Ar methods: New Mexico Geochronology Research Laboratory

Sample separation included crushing and grinding if samples were highly cemented, washing with water, sieving to appropriate grain size to concentrate the K-feldspar grains, magnetic separation, heavy liquid density separation, and optical/reflective light hand picking to concentrate sanidine grains from a mixed population of K-feldspar crystals. Hand-picking was conducted while samples were immersed in wintergreen oil while being viewed under a polarizing binocular microscope. Clear grains with no observable microtextures were sought and we estimate a ca. 90% success rate in choosing sanidine from microcline and orthoclase. Grains that yielded Precambrian ages are very likely not sanidine while grains less than ca. 300 Ma are very likely sanidine.

Crystals were irradiated in several irradiations (see below) with the majority being conducted at the TRIGA reactor in Denver, Colorado and one at the Oregon State Univ. reactor. Samples were placed in two irradiation geometries that included trays with 24 or 40 holes. All irradiations included Fish Canyon Sanidine interlaboratory standard FC-2 in a known geometry to monitor neutron flux. In all cases FC-2 was loaded in the same trays as the unknowns and there are 8 locations within a 24-hole tray and 13 in a 40-hole tray. Typically, 6 grains from each hole are analyzed and the J-value of the unknown locations is determined with a planar fit to all flux monitor locations. FC-2 is assigned an age of 28.201 Ma (Kuiper et al., 2008) and all ages are calculated with a ^{40}K decay constant of 5.463e-10 /a (Min et al., 2000).

After irradiation, monitors and unknowns were loaded into copper or stainless steel trays, evaluated and baked at temperatures between 100 and 150°C for 2 to 8 hours. Crystals were fused with a CO_2 laser using the single-crystal laser-fusion (SCLF) method. All samples were analyzed using an ARGUS VI multi-collector mass spectrometer equipped with five Faraday cups, and one electron multiplier (CDD) operated in ion-counting mode. The configuration had ^{40}Ar, ^{39}Ar, ^{38}Ar, ^{37}Ar and ^{36}Ar on the H1, Axial, L1, L2, and CDD detectors, respectively. Resistors were 10^{13} Ohms for ^{40}Ar, ^{39}Ar, ^{36}Ar and 10^{14} Ohms for ^{38}Ar. Extracted gas was cleaned with two NP 10 getters one operated at 1.6 A and one at room temperature for typically 0.5-1 minute. The cleaned gas was expanded into the mass spectrometer for isotope analysis. All data collection, analysis, and corrections were performed using either MassSpec or Pychron software and data were tabulated with Excel. Typically, isotopes of low concentration samples were collected for 280 to 600 seconds followed by 120 to 180 seconds of baseline measurement. High concentration samples (large unknown grains and FC-2) were measured using 120 seconds of isotope collection followed by 60 seconds of baseline measurement. Analyses were truncated based on various criteria to facilitate efficient data collection. For instance, relatively old grains that did not contribute significantly to MDA determination or provenance we analyzed for durations typically less than 60 seconds.

Extraction line blank behavior was relatively constant throughout this study owing to overall similar analytical protocols. Following sample tray bakeout, ^{40}Ar and associated atmospheric ^{36}Ar were elevated and decreased throughout the course of data collection that typically took about 2-3 days to complete a sample run or 221 crystals. Total static extraction time was typically 30 seconds to heat or fuse a crystal followed by 0.5-1.5 minutes of gas cleanup in the gettering system. ^{40}Ar and ^{36}Ar blanks plus mass spectrometer background were typically 2.5e-16 and 8e-19 moles, respectively at the beginning of sample run. These values fell

to about 3x less by the end of the sample run. In most cases large FC-2 grains were analyzed first because of low sensitivity to higher blanks and unknown grains were collected under lower blank conditions. To account for the time dependent blank behavior of ^{40}Ar and ^{36}Ar the blank data were typically fit as a time series using a parabolic regression of intensity versus time or linear interpolation of bracketing blank intensities. Blank uncertainty for ^{40}Ar and ^{36}Ar was typically 2-5%. For ^{39}Ar, ^{38}Ar and ^{37}Ar the blanks are not time dependent and come mainly from the mass spectrometer backgrounds. Average values for ^{39}Ar, ^{38}Ar and ^{37}Ar blanks were at or below 1e-18 moles and typically had high uncertainty of 10-50% related to detection limits of the Faraday collectors. Because of very low blanks and backgrounds relative to signal size, calculated ages are not sensitive to these corrections for the unknowns and standards. Also, during a data collection sequence, several air standards were run to monitor the ^{40}Ar/^{36}Ar detector intercalibration as well as a standard gas enriched in radiogenic ^{40}Ar and ^{39}Ar to monitor ^{40}Ar/^{39}Ar detector intercalibration. K-glass and CaF2 were included in the irradiations to determine interfering reaction correction factors.

Minimum age populations are generally defined by choosing the youngest dates that form a normal distribution as defined by the MSWD value of the distribution. The minimum age is the inverse variance weighted mean of the selected crystals and the error is the square root of the sum of $1/\sigma^2$ values. The error is also multiplied by the square root of the MSWD for MSWD greater than 1. J-error is included for all weighted mean ages and all errors are reported at 2σ unless otherwise noted. MSWD values can sometimes be high for a variety of reasons. For individual sample pits there can be measureable dispersion related to flux variations especially when pits exceed 2 mm in diameter or if grains are stacked more than 2 mm deep. Additionally, it is somewhat subjective as to which data best define the MDA and in general we include dates that maybe slightly dispersed in favor of choosing a small subset of data with a lower MSWD value.

Irradiation and Correction Factor information.

NM-283 Denver	16 hours	NM-294 Denver	16 hours
	$(^{39}Ar/^{37}Ar)_{Ca} = 0.0006928 \pm 0.0000053$		$(^{39}Ar/^{37}Ar)_{Ca} = 0.000758 \pm 0.000007$
	$(^{36}Ar/^{37}Ar)_{Ca} = 0.0002702 \pm 0.0000005$		$(^{36}Ar/^{37}Ar)_{Ca} = 0.000286 \pm 0.0000005$
	$(^{40}Ar/^{39}Ar)_{K} = 0.007439 \pm 0.000146$		$(^{40}Ar/^{39}Ar)_{K} = 0.00787 \pm 0.00058$
NM-284 Denver	16 hours	NM-300 Denver	16 hours
	$(^{39}Ar/^{37}Ar)_{Ca} = 0.0006946 \pm 0.0000017$		$(^{39}Ar/^{37}Ar)_{Ca} = 0.000709 \pm 0.0000005$
	$(^{36}Ar/^{37}Ar)_{Ca} = 0.0002606 \pm 0.0000005$		$(^{36}Ar/^{37}Ar)_{Ca} = 0.0002818 \pm 0.0000005$
	$(^{40}Ar/^{39}Ar)_{K} = 0.007531 \pm 0.000105$		$(^{40}Ar/^{39}Ar)_{K} = 0.006385 \pm 0.0003$
NM-290 Denver	12 hours	NM-304 OSU	7 hours
	$(^{39}Ar/^{37}Ar)_{Ca} = 0.00073 \pm 0.00002$		$(^{39}Ar/^{37}Ar)_{Ca} = 0.000667 \pm 0.000005$
	$(^{36}Ar/^{37}Ar)_{Ca} = 0.0002725 \pm 0.0000009$		$(^{36}Ar/^{37}Ar)_{Ca} = 0.0002750 \pm 0.000002$
	$(^{40}Ar/^{39}Ar)_{K} = 0.0088 \pm 0.0004$		$(^{40}Ar/^{39}Ar)_{K} = 0.000129 \pm 0.00008$

^{40}Ar/^{39}Ar methods: USGS Menlo Park Laboratory

Nu Noblesse mass spectrometer

^{40}Ar/^{39}Ar experiments were performed on a Nu Instruments Noblesse mass spectrometer at the U.S. Geological Survey-Menlo Park facility. The U.S. Geological Survey Noblesse features a fixed-position three detector array consisting of a high-mass faraday cup with 10^{11} Ω resistor and two discrete dynode ETP® ion counting electron multipliers (IC0 in the axial position and IC1 at the low-mass position). Electrostatic filters positioned at the entrance to each

ion counter allow for the suppression of stray ions. Two ion-optic lens arrays positioned between the magnet exit pole and the detector plane are used as a zoom lens to steer, align, and focus ion beams into the fixed detector array. At the mass range appropriate for Ar isotope measurements, the mass dispersion of the Nu Noblesse results in adjacent detectors being separated by two atomic mass units, allowing for simultaneous collection of ^{40}Ar, ^{38}Ar, and ^{36}Ar.

An advantage of the three-detector array employed by the U.S. Geological Survey Noblesse is that it has a wide dynamic range that allows Ar isotope measurements to be made on samples that vary greatly in mass and/or potassium content. Measurement of Ar isotope ratios for a given sample occurs using one of three different analytical methods depending on the size of the ^{40}Ar and ^{39}Ar signals determined on inlet (analytical methods are summarized in Data Repository Table 5). Because different samples run during the same analytical session may require the use of different analytical routines depending on their signal size, we do not vary tuning parameters (including ion-optic tuning parameters) between different cycles of a given analytical routine, or between different analytical routines. Changing mass position (i.e., peak hopping) without changing ion-optic tuning parameters will cause peak coincidence to suffer (e.g., Coble et al., 2011); however, this method does not affect the quality of the data because [1] we do not experience a degradation of peak shape by peak hopping without changing ion-optic tuning parameters, [2] multiple-collection is only performed with ^{40}Ar in the faraday detector, ^{38}Ar in ICO, and ^{36}Ar in IC1, for which ion-optic turning parameters are optimized, and [3] fluence monitors and unknowns are analyzed in the exact same manner.

Mass bias and detector efficiency correction factors

Calibration of instrumental mass bias (including mass discrimination of the source and detectors) and differences in detector efficiency is of the utmost importance when using multiple collector instruments, especially when employing a dynamic peak hopping routine (e.g., Coble et al., 2011). Precise calibration of mass bias and relative detector efficiency for the USGS Noblesse is difficult when using atmospheric argon due to the large difference in abundance of ^{40}Ar and ^{36}Ar (^{40}Ar/^{36}Ar$_{Air}$ = 298.56 ± 0.31; Lee et al., 2006). Furthermore, significant extrapolation is required to calculate correction factors for ^{40}Ar/^{39}Ar from measured ^{40}Ar/^{36}Ar on atmospheric argon (e.g., Renne et al., 2009). To circumvent this problem, calibration of instrumental mass bias and relative detector efficiently for the Noblesse is done using a gas mixture produced by the U.S. Geological Survey and Stanford University with a known ^{40}Ar/^{39}Ar, ^{38}Ar/^{39}Ar, and ^{36}Ar/^{39}Ar (hereafter referred to as USGS-SU-MG). For each analytical session ion-optic tuning, source, and detector settings are tuned using 1 shot of the USGS-SU-MG with ^{40}Ar measured in the high mass faraday detector, ^{38}Ar in ICO, and ^{36}Ar in IC1 such that signal intensity, peak shape, and peak coincidence are optimized. Following tuning, correction factors are determined for ^{40}Ar/^{39}Ar, ^{38}Ar/^{39}Ar, and ^{36}Ar/^{39}Ar by measuring splits of the USGS-SU-MG in the same cup configurations as employed for unknown analyses and comparing the measured ^{40}Ar/^{39}Ar, ^{38}Ar/^{39}Ar, and ^{36}Ar/^{39}Ar to the known Ar-isotope ratios of the USGS-SU-MG. For example, the ^{40}Ar/^{39}Ar correction factor for method 2 (see Data Repository Table 5) is calculated as follows:

$$CF_{40Ar(Farady)/39Ar(IC0)} = \frac{\left[\frac{^{40}Ar_{Farady}}{^{39}Ar_{IC0}}\right]_{measured}}{\left[\frac{^{40}Ar}{^{39}Ar}\right]_{accepted}}$$ (1)

Correction factors are measured at the beginning and end of each analytical session. To date no drift in correction factors has been observed over the course of a given analytical session. These correction factors are then applied to measured isotope ratios for fluence monitors and unknowns by dividing the measured Ar isotope ratios by the relevant correction factor. For example, the corrected $^{40}Ar/^{39}Ar$ for method 2 (see Data Repository Table 5) is calculated as follows:

$$^{40}Ar/^{39}Ar_{corrected} = \frac{\left[\frac{^{40}Ar_{Farady}}{^{39}Ar_{IC0}}\right]_{measured}}{CF_{40Ar(Farady)/39Ar(IC0)}}$$ (2)

Because the USGS-SU-MG does not contain ^{37}Ar due to its short half-life of 35.1 days, the $^{37}Ar/^{39}Ar$ correction factor cannot be measured directly. Instead, the $^{37}Ar/^{39}Ar$ correction factor is calculated by linear extrapolation of the $^{38}Ar/^{39}Ar$ correction factor, which in all analytical methods is measured on the same detectors as $^{37}Ar/^{39}Ar$ (Data Repository Table 5).

$$CF_{37/39} = 1 - (1 - CF_{38/39}) * 2$$ (3)

Uncertainties in the correction factors include counting statistics and the uncertainty in the Ar isotope compositions of the USGS-SU-MG, and these uncertainties are propagated when calculating Ar isotope ratios of fluence monitors and unknowns.

Dead time corrections and detector linearity

An important consideration when using ion counting systems is electronic dead time and the nonlinear behavior of the detectors with changing signal size. To account for these effects, we apply a correction factor that accounts for both dead time and any nonlinearity in the detectors following Coble et al. (2011). To calculate these correction factors, we measure the $^{36}Ar/^{39}Ar$ of the USGS-SU-MG (true value of 0.3773 ± 0.0014) on each ion counting detector over a range of signal intensities from 5.6×10^4 cps to 9.2×10^5 cps on ^{39}Ar and 2.1×10^4 cps to 3.4×10^5 cps on ^{36}Ar. We assume that the measured $^{36}Ar/^{39}Ar$ of the USGS-SU-MG should not change as a result of variation in the signal size. Using the standard dead time correction ($CPS_{corr} = CPS_{meas}/[1-CPS_{meas}*\tau]$), where CPS_{meas} is the measured signal intensity, CPS_{corr} is the dead time corrected signal intensity, and τ is the value for dead time in nanoseconds (Fahey, 1998), we iteratively vary the dead time for each detector until the MSWD of the dead time corrected $^{36}Ar/^{39}Ar$ for each detector measured over the entire range of signal sizes is minimized. Using this approach, the dead times for IC0 and IC1 are 25.6 ns and 25.5 ns, respectively. An uncertainty of 3 ns is propagated when doing dead time corrections.

Analytical considerations and age calculation

$^{40}Ar/^{39}Ar$ ages were measured for single sanidine crystals by laser total fusion using a CO_2 laser connected to a Nu Instruments Noblesse mass spectrometer. For laser total fusion analyses of fluence monitors and sanidine grains of unknown age, argon was extracted from the sanidine grains in a single heating step (i.e., total fusion) using a New Wave CO_2 laser. Extracted Ar was exposed to a 4 A tungsten filament and two SAES ST-172 getters (one operated at 300ºC, and one at room temperature) to remove active gasses. Measured signal intestines for fluence monitors, unknowns, and USGS-SU-MG (projected to time zero) are corrected for line blanks and for baseline electronic noise measured by deflecting the ion beam vertically into the wall of the mass spectrometer. $^{40}Ar/^{39}Ar$ ages are calculated relative to Bodie Hills sanidine with an age of 9.797 ± 0.0031 Ma, equivalent to Fish Canyon sanidine at 28.1053 ± 0.0124 Ma, and using the decay constants recommended by Steiger and Jäger (1977). Uncertainties for reported $^{40}Ar/^{39}Ar$ ages include propagated uncertainties in counting statistics, J values, and correction factors. For the purpose of this manuscript we have recalculated all ages using the decay constants recommended by Min et al. (2010) and relative to Fish Canyon sanidine at 28.201 Ma (Kuiper et al., 2008).

University of Oklahoma Paleomagnetic Analytical Details and Results

Analytical methods

Oriented slabs were collected in the field and specimens were dry cut using a band saw due to the friable nature of the slabs. Thermal and alternating field (AF) demagnetization of the samples was performed with a 2G cryogenic magnetometer. Alternating field demagnetization consisted of 12 steps (10mT each) from 10mT to 120mT. Thermal demagnetization subjected samples to a total 20 steps, with 100°C steps from 100° to 300° C, and 25 steps from 325° to 700° C. A test set (<20) of samples underwent low temperature demagnetization (LTD) treatment (3 steps of liquid nitrogen submersion, return to room temperature, and then measurement of the NRM) to remove contamination from the Modern field component that is held in multi-domain magnetite grains (Dunlop and Argyle, 1991).

Magnetization components from all sites were determined using orthogonal vector projections (Zijderveld, 1967) and equal area projections. Super IAPD (http://www.geodynamics.no/resources.html) was used for principal component analysis (Kirschvink, 1980) to determine magnetic components. Sample sites were picked utilizing primary component analysis to distinguish ChRMs and then classified according to the trend and reliability of demagnetized components. Sites in which the ChRM decayed linearly to the origin were classified as Class "A" data. Sites in which the ChRM clustered near the origin were defined as Class "B" data. Polarity was interpreted in both Class A & B sites from the inclination of the ChRM, where a negative inclination indicates a reversed polarity and a positive inclination indicates a normal polarity. Polarities that displayed irregular or flipped declination and inclination data were labeled as ambiguous. Sites that displayed a rapid demagnetization on Zijderveld plots or showed signs of overlapping components were defined as Class "C" data. Polarity was determined in these sites using a combination Zijderveld plots, demagnetization curve trends and equal area projections. Sites in which no polarity could be determined due to overlapping components or weak magnetization were defined as Class "D" data.

Results from the HighWall Wash site

A total of 36 samples from 11 sample sites (Data Repository Table 6) were used to determine polarity of the Lost Cabin beds from the Highwall Wash ash site (Data Repository Figure 1), where the ash has been dated at 5.35 ± 0.07 Ma. Samples were collected above (HWW 8-12), below (HWW 1-6), and within the ash (HWW 7). The samples were demagnetized using both alternating field (AF) and thermal demagnetization techniques (see methods). Data Repository Table 6 shows the demagnetization results from the Highwall Wash locality. In summary, below the ash, sites HWW 5 and 6 show predominately reverse polarities, while above the ash, sites HWW 8, 9, 11, and 12 show normal polarities. Site HWW 7, within the ash, shows reversed polarity. The remaining sites show ambiguous results, as the magnetic mineralogy is complex (see below). Figure 2 shows representative orthogonal projection diagrams from both reverse (HWW8-1) and normal (HWW11-1) specimens.

The ChRM was isolated only through AF demagnetization; thermal generally yields ambiguous and noisy results. AF decay shows a ChRM that is present from ~20mT-90mT. Not all AF decay of the samples reaches the origin, which implies there may be more than one magnetic carrier present. Rock magnetic experiments show that the ChRM in the HWW is likely held in pyrrhotite. Figure 4 shows isothermal remanent magnetization (IRM) acquisition and decay curves for HWW samples. The samples are nearly saturated by 250mT, and tri-axial decay shows that nearly full decay has occurred by 300°C. There is a high-coercivity component likely present in the samples as evidenced by decay past 300°C, although this component does not carry the ChRM. For the HWW locality, the ChRM is interpreted to be held in pyrrhotite. Pyrrhotite has a low coercivity which is dependent on grainsize and varies from 55-75mT for grain sizes in the 1-10μm range (Roberts et al., 2006), which is small enough to hold a remanent magnetization (see Fig. 2). Thermal demagnetization was performed in 100° steps up to 300°C and in 25°C steps to 600°C. The large step-size was inadequate to isolate a pyrrhotite component in thermal demagnetization, since the Curie temperature of pyrrhotite is 320°C.

Data Repository Figure 3 is an equal area plot of the Highwall Wash samples showing both the normal and reverse specimens with their corresponding group means (plus signs) and associated errors (ellipse). Also plotted are the means of the positive reversal test from the Lost Cabin beds at the Lost Cabin Wash sample site. Although the reversal test fails at the Highwall Wash ash site, likely because of the small number of samples that hold the reverse ChRM, the means overlap with the positive reversal test within Lost Cabin beds at Lost Cabin Wash. Based on this, an interpreted reversal is likely captured within this site, directly above the ash, at an elevation of 322 m above sea level (asl), and is interpreted as the same reversal interval seen in Lost Cabin Wash (at 320.9 m asl)(Schwing, 2019), representing the transition from the C3r subchron to C3n.4n (Thvera) subchron of the Gilbert Chron (GPTS: Ogg et al., 2012 and Channell et al., 2020). A larger sample size is needed at Highwall Wash to determine if the reversal is present and statistically valid.
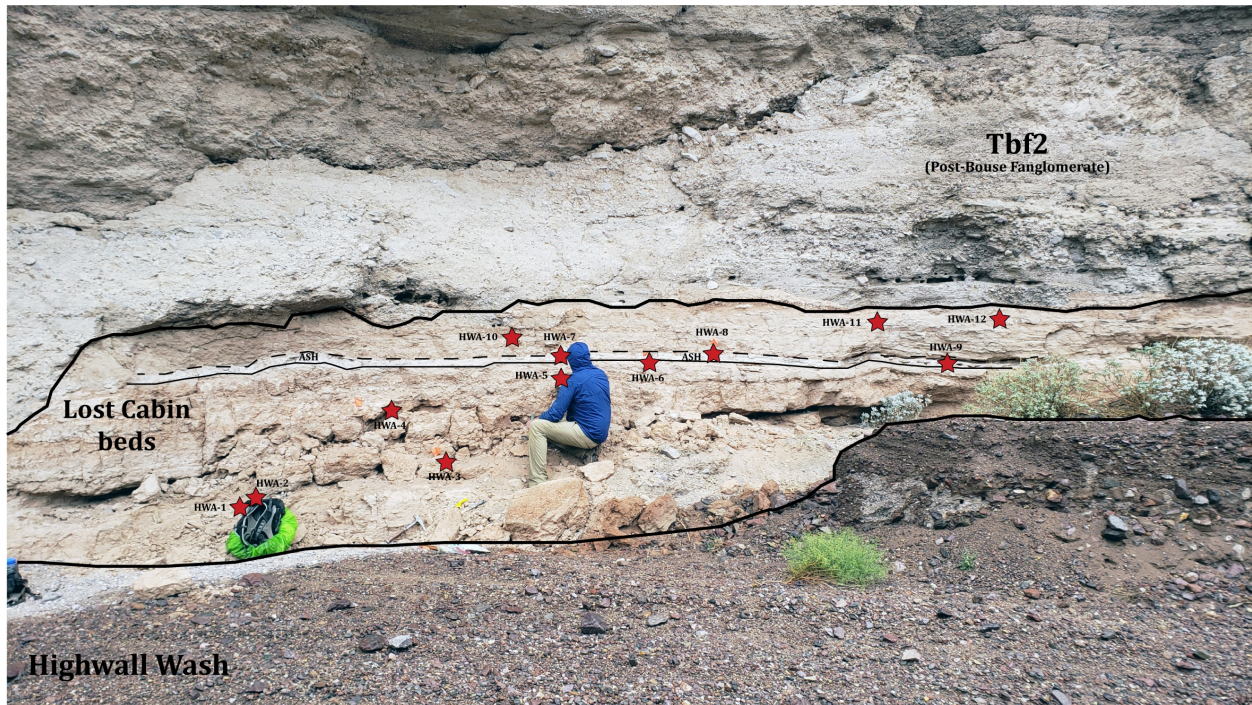
Data Repository Figure 1: Sample site localities at the Highwall Wash Ash Site. Dashed line shows interpreted reversal site which lies directly above the ash bed in sample HWW-7.
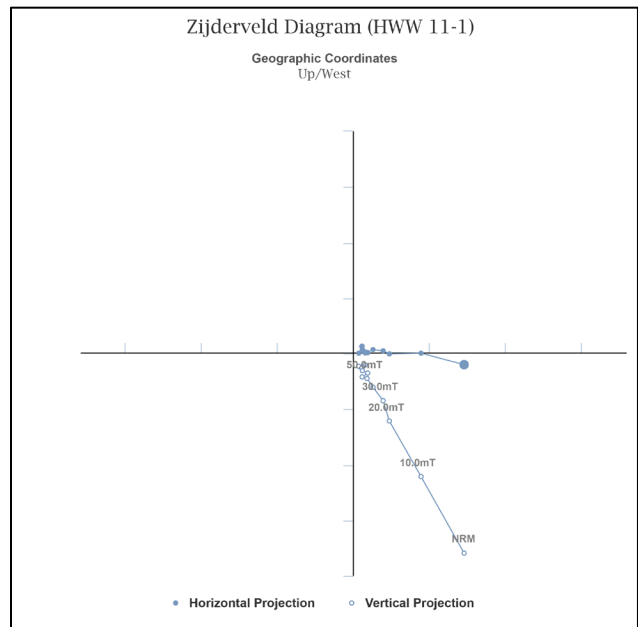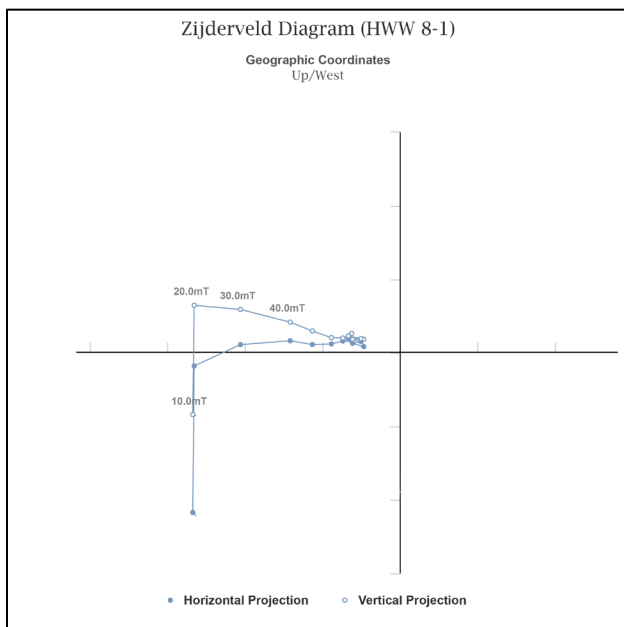
Data Repository Figure 2: Orthogonal projection diagrams (Zijderveld, 1967) showing AF decay of both reverse (HWW8-1) and normal (HWW11-1) samples. Open (closed) circles represent inclination (declination). The ChRM decays from ~20mT-90mT in most samples.
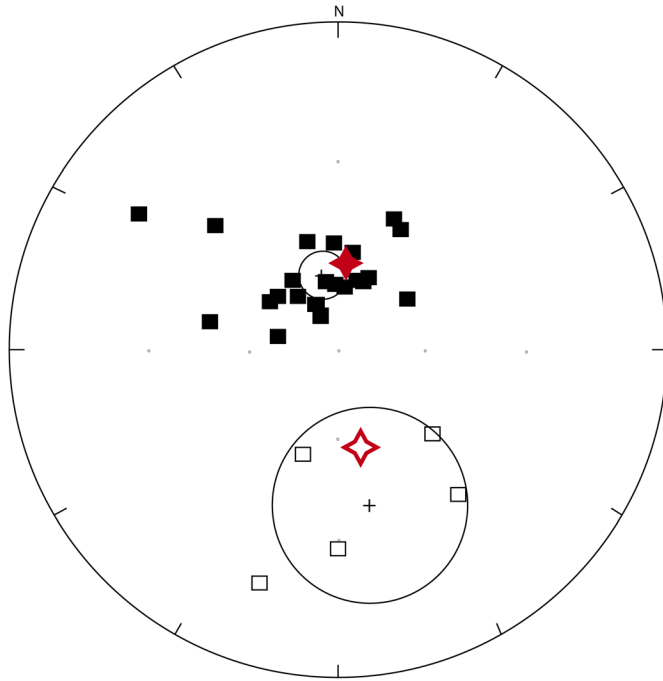
Data Repository Figure 3: Equal are plot of all reverse (open boxes) and normal (closed boxes) sample directions from Highwall Wash. The plus signs represent the mean of each grouping and the associated error ellipses. The red diamonds represent the mean directions (error too small to plot) of the reverse (open red diamond) and normal (solid red diamond) groupings from the positive reversal test performed on the Lost Cabin Wash bed samples (Schwing, 2019).

IRM Acquisition Curve HWW8-1
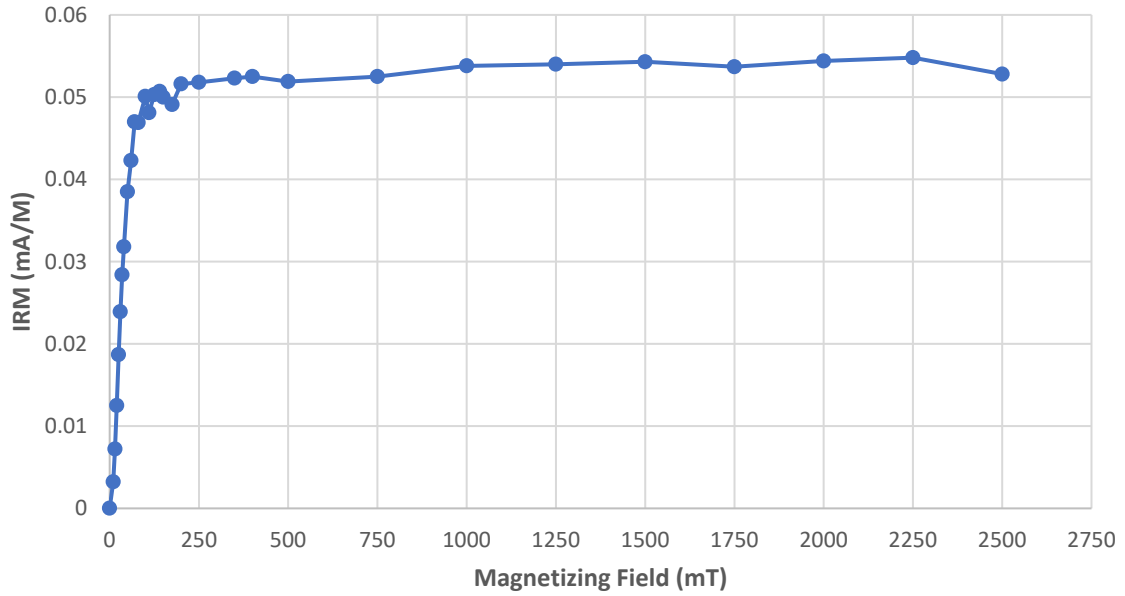
TriAxial Decay Curves HWW 8-1
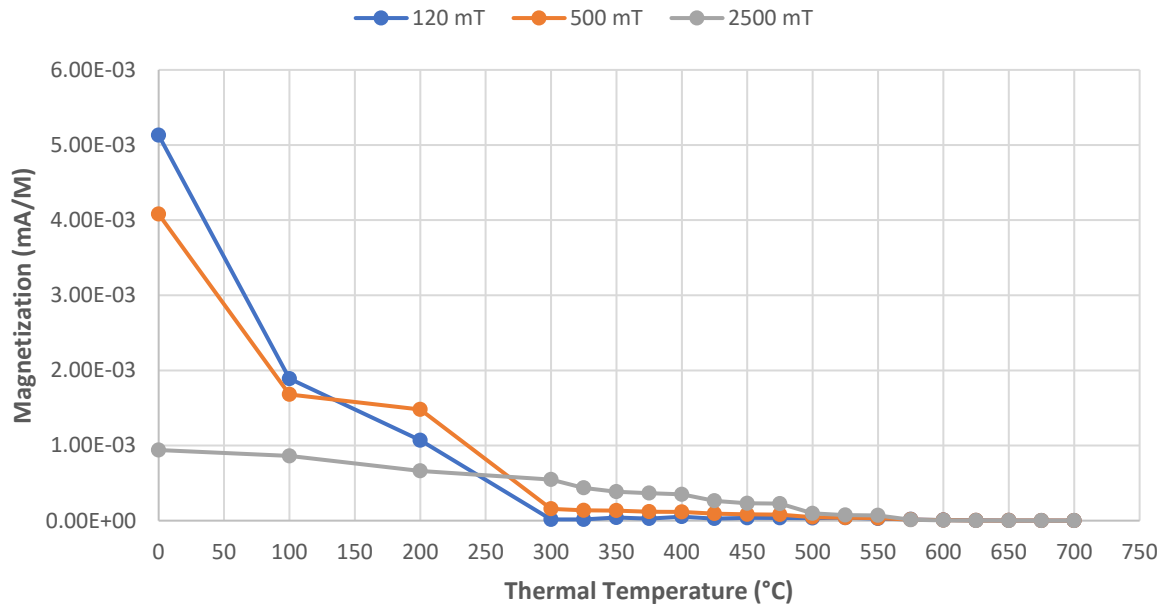
Data Repository Figure 4: IRM Acquisition and triaxial decay curves of HWW 8-1. IRM saturation values are in milliamps/meter (mA/M), with increasing field values measured in milliTesla (mT). Triaxial decay magnetic components are divided into soft (120mT), medium (500mT), and hard (2500mT) and were thermal demagnetized up to 700°C.

REFERENCES

Channell, J.E.T., Singer, B.S., and Jicha, B.R., 2020, Timing of Quaternary geomagnetic reversals and excursions in volcanic and sedimentary archives: v. 228, doi:10.1016/j.quascirev.2019.106114.

Coble, M.A., Grove, M., and Calvert, A.T., 2011, Calibration of Nu-Instruments Noblesse multicollector mass spectrometers for argon isotopic measurements using a newly developed reference gas: Chemical Geology, v. 290, p. 75–87, doi:10.1016/j.chemgeo.2011.09.003.

Dunlop, D. J., and Argyle, K. S., 1991, Separating multidomain and single-domain-like remanences in pseudo-single-domain magnetites (215–540 nm) by low-temperature demagnetization: Journal of Geophysical Research, v.96, p. 2007-2017.

Fahey, A.J., 1998, Measurements of dead time and characterization of ion counting systems for mass spectrometry: Review of Scientific Instruments, doi:10.1063/1.1148796.

Kirschvink, J. L.,1980, The least-squares line and plane and the analysis of palaeomagnetic data: Geophysical Journal of the Royal Astronomical Society, v.62, p. 699-718.

Kuiper, K.F., Deino, A., Hilgen, F.J., Krijgsman, W., Renne, P.R., and Wijbrans, J.R., 2008, Synchronizing Rock Clocks of Earth History: Science, v. 320, p. 500–504, doi:10.1126/science.1154339.

Lee, J.Y., Marti, K., Severinghaus, J.P., Kawamura, K., Yoo, H.S., Lee, J.B., and Kim, J.S., 2006, A redetermination of the isotopic abundances of atmospheric Ar: Geochimica et Cosmochimica Acta, v. 70, p. 4507–4512, doi:10.1016/j.gca.2006.06.1563.

Min, K., Mundil, R., Renne, P.R., and Ludwig, K.R., 2000, A test for systematic errors in 40Ar/39Ar geochronology through comparison with U/Pb analysis of a 1.1-Ga rhyolite: Geochimica et Cosmochimica Acta, doi:10.1016/S0016-7037(99)00204-5.

Ogg, J.G., 2012, Geomagnetic Polarity Time Scale:, doi:10.1016/B978-0-444-59425-9.00005-6.

Renne, P.R., Cassata, W.S., and Morgan, L.E., 2009, The isotopic composition of atmospheric argon and 40Ar/39Ar geochronology: Time for a change? Quaternary Geochronology, doi:10.1016/j.quageo.2009.02.015.

Roberts, A.P., Liu, Q., Rowan, C.J., Chang, L., Cravall, C., Torrent, J., and Horng, C., 2006, Characterization of hematite (a-Fe2O3), goethite (a-FeOOH), greigite (Fe3S4), and pyrrhotite (Fe7S8) using first-order reversal curve diagrams: Journal of Geophysical Research, v. 111, B12S25, doi:10.1029/2006JB004529

Schwing, J., 2019, Magnetostratigraphy of the Pre-Colorado River integration Lost Cabin beds, Cottonwood Valley, Arizona [M.S. thesis]: Norman, University of Oklahoma, 112 p.

Steiger, R.H., and Jäger, E., 1977, Subcommission on geochronology: Convention on the use of decay constants in geo- and cosmochronology: Earth and Planetary Science Letters, v. 36, p. 359–362, doi:http://dx.doi.org/10.1016/0012-821X(77)90060-7.

Zijderveld, J.D.A., (1967). A.c. demagnetization of rocks: analysis of results, *in* Collinson, D.E. et al., eds., Methods in Paleomagnetism: New York, Elsevier Science, p. 254-286.